
Pushing the Boundaries of State Space Models for Image and Video Generation

Yicong Hong¹ Long Mai¹ Yuan Yao^{1,2} Feng Liu¹

¹Adobe Research, ²University of Rochester

Project Page: <https://yiconghong.me/HTH>

Abstract

While Transformers have become the dominant architecture for visual generation, linear attention models, such as the state-space models (SSM), are increasingly recognized for their efficiency in processing long visual sequences. However, the essential efficiency of these models comes from formulating a limited recurrent state, enforcing causality among tokens that are prone to inconsistent modeling of N-dimensional visual data, leaving questions on their capacity to generate long non-causal sequences. In this paper, we explore the boundary of SSM on image and video generation by building the largest-scale diffusion SSM-Transformer hybrid model to date (5B parameters) based on the sub-quadratic bi-directional Hydra and self-attention, and generate up to 2K images and 360p 8 seconds (16 FPS) videos. Our results demonstrate that the model can produce faithful results aligned with complex text prompts and temporal consistent videos with high dynamics, suggesting the great potential of using SSMs for visual generation tasks.

1. Introduction

In recent years, we have witnessed remarkable advancements in industrial-scale visual generation, spanning images (Esser et al., 2021; Dhariwal & Nichol, 2021; Rombach et al., 2022; Saharia et al., 2022; Peebles & Xie, 2023; Chang et al., 2023; Ruiz et al., 2023; Podell et al., 2023), videos (Yan et al., 2021; Ho et al., 2022; Blattmann et al., 2023; Girdhar et al., 2023; Kondratyuk et al., 2023; Bar-Tal et al., 2024), 3D assets (Hong et al., 2023; Li et al., 2023; Xu et al., 2023; Wang et al., 2024b; Watson et al., 2024), embodied interactions (Wu et al., 2023; Yang et al., 2023a; Du et al., 2024; Cheang et al., 2024; Yang et al., 2024), and more. Central to many of these approaches is Transformer architecture (Vaswani et al., 2017), which serves as the core model backbone. Transformers, powered by the self-

attention token mixing mechanism, effectively capture the relationships among visual tokens to produce realistic visual content and have proven highly scalable (Dosovitskiy, 2020; Dehghani et al., 2023). However, the quadratic computational complexity of Transformer models poses significant efficiency challenges, leading to dramatic slowdowns when processing long token sequences and making them impractical to common users (Kitaev et al., 2020; Wang et al., 2020; Beltagy et al., 2020).

Meanwhile, there has been a surge in linear complexity models (LCM) (Katharopoulos et al., 2020; Choromanski et al., 2020; Shen et al., 2021; Qin et al., 2022; Yang et al., 2023b); large models built based on RetNet (Sun et al., 2023), RWKV (Peng et al., 2023), GLA (Yang et al., 2023b), and Mamba (Gu & Dao, 2023; Dao & Gu, 2024) have demonstrated performance comparable to Transformers across a variety of natural language processing tasks while achieving superior inference time speed. This success inspires recent research such as building linear complexity visual generative models (Yan et al., 2023; Hu et al., 2024; Fei et al., 2024; Yang et al., 2023b; Zhu et al., 2024) and exploring Transformer-to-LCM distillation (Wang et al., 2024a; Bick et al., 2024; Liu et al., 2024). Despite their efficiency advantages, these methods often fail to produce visual outputs with the same quality as Transformer models. An essential reason behind this is that most of the LCMs are formulated as a stateful model that enforces causality on the input (tokens), which does not align with the non-causal N-dimensional nature of visual data. As a result, many recent generative visual LCMs implement multi-directional scans and preserve self-attention (Gao et al., 2024; Zhang et al., 2024c; Fei et al., 2024; Hu et al., 2024; Chen et al., 2024b; Yi et al., 2024), which enlarges the receptive field of each token across layers. However, those models and experiments mostly only deal with short visual sequences (*e.g.*, low-res images), which cannot reflect the memory limitation or justify the expressiveness of LCMs (Jelassi et al., 2024; Merrill et al., 2024). On the other hand, several works attempt to build non-casual LCMs by squeezing all visual tokens into the fix-sized state at once (Liu et al., 2024; Xie et al., 2024) or establishing a state representation that shares the same information with all the tokens (Shi et al., 2024); despite

²Intern at Adobe Research.



Figure 1. Text-to-1K/2K+ image generation results of our Hydra-Transformer Hybrid model. The resolution of each sample is displayed in the bottom-right corner. Text prompts and additional results are provided in the Appendix. Please zoom in for a clearer visualization.

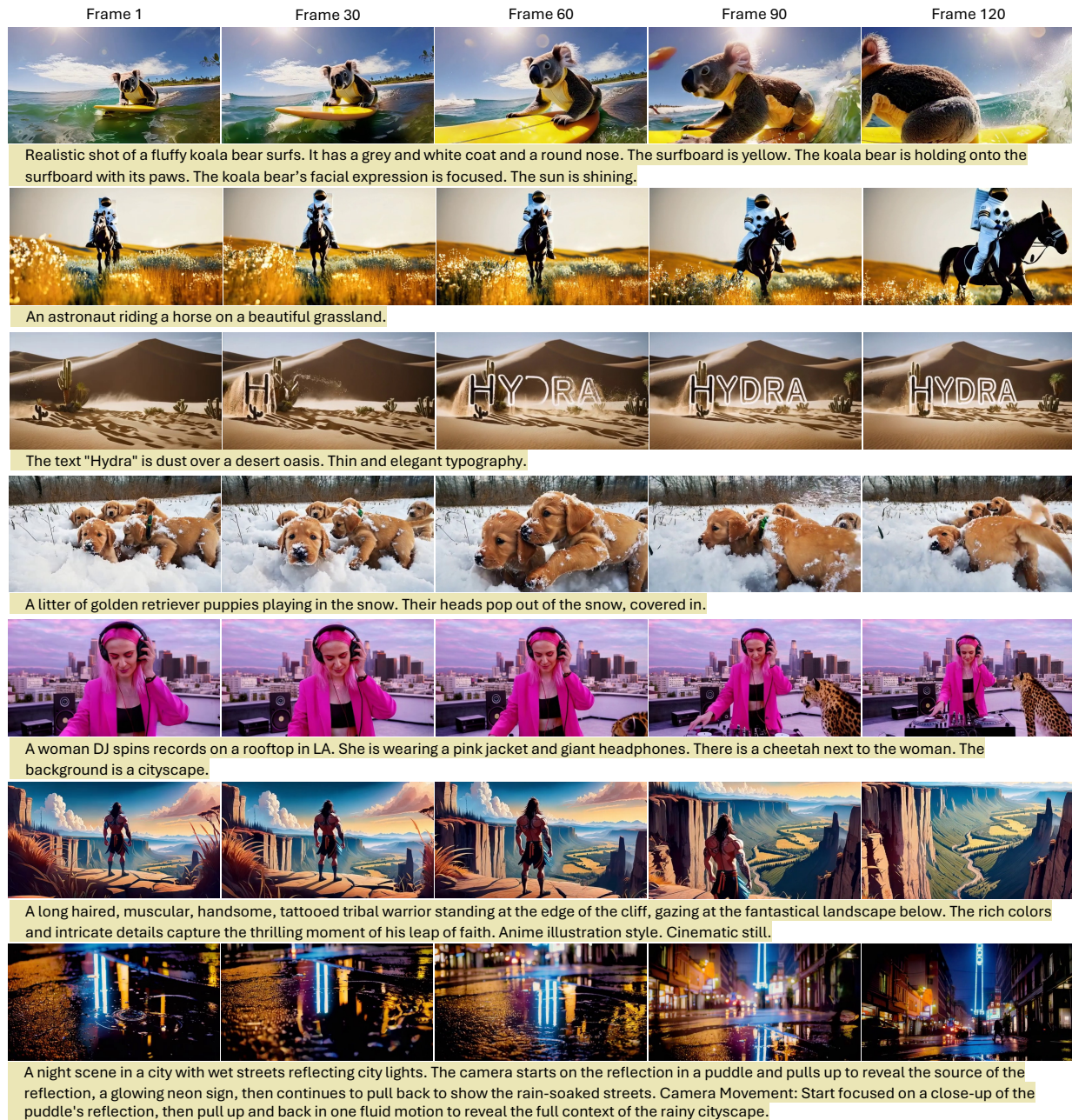


Figure 2. Text-to-360p 128 frames video generation results produced by our Hydra-Transformer Hybrid model. More results are provided in the Appendix. Please zoom in for a clearer visualization.

encouraging results on image generation, our preliminary experiments show that these methods struggle with complex text prompts or video generation, where the latter requires learning much more complicated spatiotemporal patterns.

In light of the above, this paper takes an empirical approach to explore the boundary of State Space Models (SSM) in long-sequence visual generation with diffusion. Specifically, we apply the best-performing bi-directional SSM, Hydra, and follow the previous research to build a Hydra-and-Transformer Hybrid model (HTH). We consider the

simplest horizontal and vertical raster scan patterns while focusing on scaling the model to 5B parameters for generating up to 2K images (1440×2560) and 360p 8-second videos (16 FPS), respectively. Compared to 2D images, video data has an extra dimension which introduces large scanning complexity to the SSM. Here, to adapt the image-trained HTH base model for video generation, we propose a simple but effective method that directly changes the scanning order of some layers to temporal-first, forcing these layers to learn the temporal evolution of tokens at the same 2D position. Our final results reveal that the HTH model

effectively generates faithful outputs that align with complex text prompts while producing temporally consistent and highly dynamic videos, highlighting the potential of sequential linear complexity models in visual generation.

2. Background

2.1. Selective State Space Models

The recently proposed selective state space models (S4, *e.g.*, Mamba (Gu & Dao, 2023; Dao & Gu, 2024)) formulate a sequential transformation that maps a sequence $x_t \in \mathbb{R}^d \mapsto y_t \in \mathbb{R}^d$ through an implicit latent state $h_t \in \mathbb{R}^N$. Specifically, S4 models are defined with four input-dependent parameters, Δ_t , \mathbf{A}_t , \mathbf{B}_t , and \mathbf{C}_t , which their discrete form can be generally expressed as

$$h_t = \overline{\mathbf{A}}_t h_{t-1} + \overline{\mathbf{B}}_t x_t \quad y_t = \mathbf{C}_t^\top h_t \quad (1)$$

where Δ_t controls the preservation of the current state, and $\overline{\mathbf{A}}_t$ and $\overline{\mathbf{B}}_t$ are produced by a discretization rule such as via the Zero-Order Hold as

$$\begin{aligned} \overline{\mathbf{A}}_t &= \exp(\Delta_t \mathbf{A}_t) \\ \overline{\mathbf{B}}_t &= (\Delta_t \mathbf{A}_t)^{-1} (\exp(\Delta_t \mathbf{A}_t) - \mathbf{I}) \cdot \Delta_t \mathbf{B}_t \end{aligned} \quad (2)$$

Referring to the state-space duality (Dao & Gu, 2024; Hwang et al., 2024), SSMs present a matrix transformation form for a $(\overline{\mathbf{A}}, \overline{\mathbf{B}}, \mathbf{C})$ -parameterized semiseparable matrix $\mathbf{M}_\theta \in \mathbb{R}^{(T,T)}$, where T indicates the length of input sequence $\mathbf{X} \in \mathbb{R}^{(T,d)}$. Concisely, we can view the sequential transition

$$\begin{aligned} y_t &= \sum_{s=0}^t \mathbf{C}_t^\top \overline{\mathbf{A}}_{t:s}^\times \overline{\mathbf{B}}_s x_s \\ \overline{\mathbf{A}}_{i:j}^\times &= \begin{cases} \prod_{k=j+1}^i \overline{\mathbf{A}}_k, & i > j \\ 1, & i = j \end{cases} \end{aligned} \quad (3)$$

as

$$\mathbf{Y} = \mathbf{M}_\theta \mathbf{X} \quad (4)$$

where $m_{ij} = \mathbf{c}_i^\top \overline{\mathbf{A}}_i \cdots \overline{\mathbf{A}}_{j+1} \overline{\mathbf{b}}_j$ are the (i, j) -entries that fill the lower-triangular part of \mathbf{M}_θ .

2.2. Hydra: Bidirectional SSM

A core limitation of the above SSM formulation lies in its inherent causality, which constrains its ability to model N -dimensional visual data effectively. To address this issue while allowing the model to possess strong expressiveness and leverage sub-quadratic matrix multiplication algorithms, the Hydra bidirectional SSM is introduced (Hwang et al., 2024). Hydra employs a quasiseparable matrix as the token mixer and is implemented using the Mamba-2 framework (Dao & Gu, 2024).

Specifically, the quasiseparable matrix (QS) in Hydra is formed by combining two semiseparable matrices (SS) cor-

responding to forward and reverse sequence modeling:

$$QS(\mathbf{X}) = \hat{s}(SS(\mathbf{X})) + \hat{f}(\hat{s}(SS(\hat{f}(\mathbf{X})))) + \mathbf{D}\mathbf{X} \quad (5)$$

where \mathbf{D} denotes the learnable diagonal parameters of the quasiseparable matrix. \hat{f} and \hat{s} are two non-parameterized operations; \hat{f} reverses the input sequence, \hat{s} shifts the sequence right by one position and pads the beginning with zero. As claimed and empirically justified in the Hydra paper, the above formulation of a quasiseparable matrix is strictly more expressive than existing addition-based bidirectional SSMs. We refer readers to the original paper for proof of the derivation (Hwang et al., 2024).

3. Method

We present our Hydra-Transformer Hybrid model (HTH), a diffusion framework for text-guided image and video generation (Figure 3). Similar to the Diffusion Transformer (Peebles & Xie, 2023), we consider the simplest network components and architecture to establish a general and highly scalable large model. Inspired by recent study (Waleffe et al., 2024), we effectively combine the Hydra state space model and self-attention by simply switching the token mixer across layers to allow our HTH to benefit from both efficient processing and global interaction. We specify the network architecture of HTH in §3.1 and §3.2, and the adaptation of T2I to T2V training in §3.3.

3.1. HTH Architecture

Data Encoders The framework starts with textual and visual encoders for preprocessing the text prompt and its corresponding image or video. Similar to existing approaches (Ho et al., 2022; Kondratyuk et al., 2023; Sun et al., 2024; Black Forest Labs, 2024), we adopt the T5 language model (Raffel et al., 2020), specifically FLAN-T5-XXL (Chung et al., 2024), to acquire textual representations. We compress raw visual input into a low-dimensional continuous latent space using a 3D VAE adapted from MAGVIT-v2 (Yu et al., 2023). The VAE can encode 2D images and incorporate motion encoding from video frames. Both VAEs produce 12-channel latent representations with an $8 \times$ spatial compression and $\frac{16}{5} \times$ temporal compression.

Denosing Model As visualized in the top-left of Figure 3, the denosing model in HTH is formed by stacking N blocks of residual-connected and pre-normed (Xiong et al., 2020; Lei Ba et al., 2016) cross-attention, token mixer, and feed-forward layers. Starting with the cross-attention layer, it attends the input token sequence (*i.e.*, the noised image/video latents) to the textual representations to acquire language guidance. Then, the token mixer layer, either Hydra or self-attention, models and coordinates the interactions among the visual latents, followed by a feed-forward layer to in-

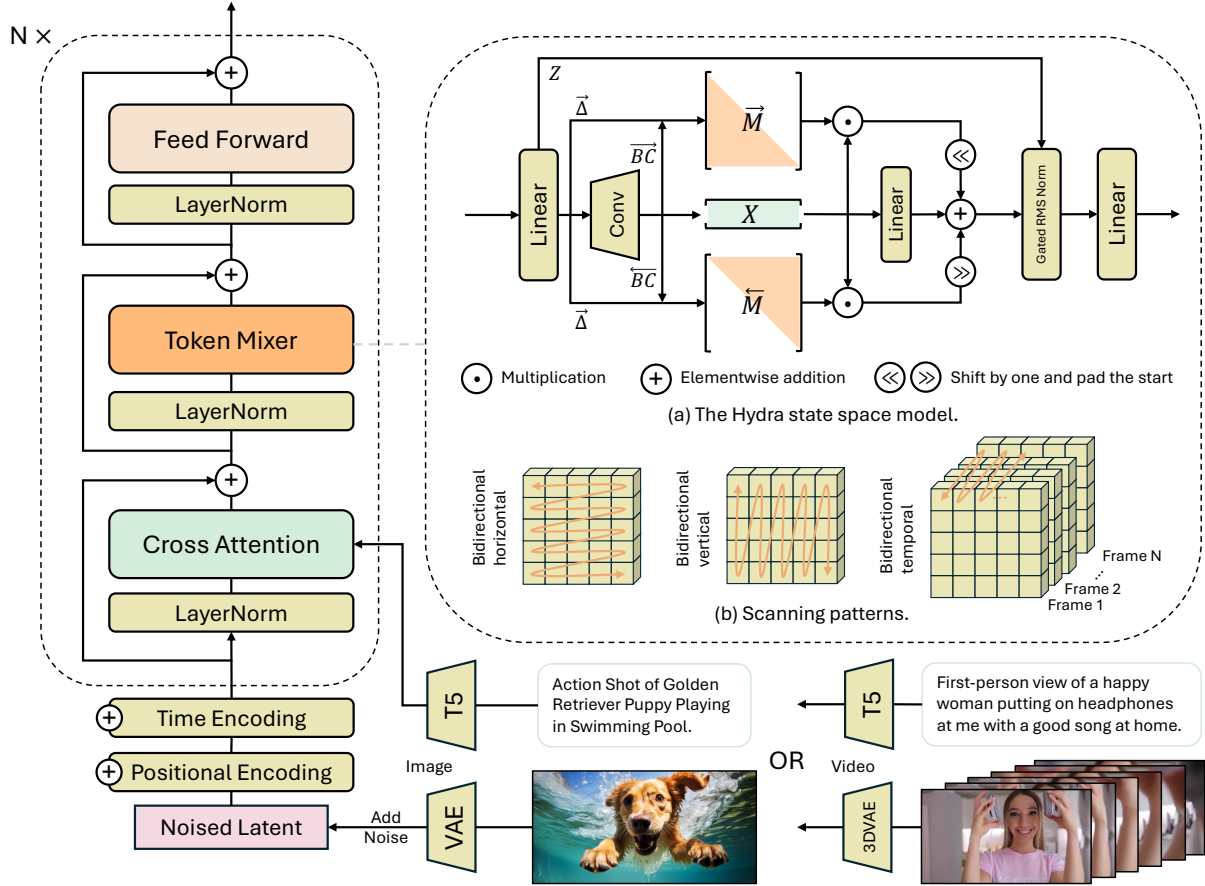


Figure 3. Illustration of our diffusion Hybrid Hydra (HTH) model for image and video generation. The architecture consists of N stacked blocks, each comprising a cross-attention layer, a token mixer, and a feed-forward network. (a) The token mixer can be implemented as either the Hydra state space model or self-attention. (b) For image data, we use horizontal and vertical bidirectional raster scans on tokens, and for video data, an additional bidirectional temporal scan is applied.

corporate general knowledge. We choose Hydra among the SSM variants due to its efficient implementation of a non-causal model with superior expressiveness (Hwang et al., 2024). We refer to Appendix B.1 for comparison between unidirectional SSM, bidirectional SSM, the state-sharing VSSD (Shi et al., 2024), self-attention, and Hydra.

Scanning Patterns Due to the bi-directional sequential nature of Hydra, the processed tokens are biased towards a higher correspondence to the adjacent tokens in the flattened 1D sequence, which contradicts the structure continuity of 2D and 3D visual data. To enlarge the receptive field of tokens, we alternate the scanning pattern between each of the two consecutive Hydra blocks. As shown in Figure 3, we only consider two bi-directional raster scans, via either a horizontal or a vertical path. While previous research has explored other scanning patterns in various domains (Zhang et al., 2024b; Xu et al., 2024), their impact on large-scale diffusion SSMs remains unclear. Experimenting with different scanning patterns falls outside the scope of this paper and is left for future work.

Conditioning Mechanisms We leverage simple but effective methods to incorporate the diffusion and textual conditions. For the learnable diffusion timestep encoding, we add it directly to the noised latents once, before passing them to the first HTH layer. In contrast to the Adaptive LayerNorm applied in DiT (Peebles & Xie, 2023), this approach significantly saves the parameters and computation of the model. For the text prompts, we use a cross-attention layer to introduce semantic guidance from the text tokens to the visual tokens. Exploring other possible design choices, such as formulating in-context multimodal SSM (*i.e.*, prepending text tokens to visual tokens, and initiating scanning from the text tokens (Hu et al., 2024)), is out of the scope of this paper. We leave this exploration for future work.

3.2. Hydra and Self-Attention Integration

Inspired by existing works that combine SSM layers and Transformer layers (Zuo et al., 2022; Waleffe et al., 2024; Lieber et al., 2024; Fei et al., 2024; Ziwen et al., 2024; Wang et al., 2024a) as well as other linear hybrid RNN

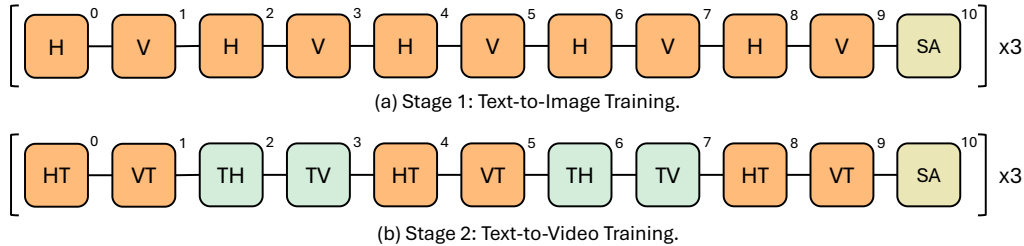


Figure 4. Illustration of the model adaptation from state 1 (T2I) to state 2 (T2V). For each set of 11 blocks in our HTH model, we change the scanning pattern of certain Hydra layers from spatial-major to temporal-major scan when processing video data.

networks (Botev et al., 2024; De et al., 2024), we create our hybrid model that enjoys the efficiency advantage and global interaction from SSM and self-attention, respectively. As shown in Figure 4(a), our HTH model consists of a total $N=33$ blocks, with each set of 11 blocks containing 10 Hydra blocks followed by a final self-attention block. We formulate HTH to have a high Hydra-to-Transformer ratio (30:3) to exploit the modeling capacity of SSMs and preserve efficiency.

3.3. T2I to T2V Adaptation

Following the common multi-stage training strategy (Hong et al., 2022; Blattmann et al., 2023; Girdhar et al., 2023; Bartal et al., 2024), we first train a base T2I model before applying video data, allowing the T2V HTH to inherit the rich semantics and high visual quality learned from abundant images. However, video data introduces an extra dimension that significantly increases the modeling distance between spatially or temporally adjacent tokens and demands additional temporal-scanning SSMs to model the frame-wise consistency and evolution. Our early empirical results indicate that neither directly using the stage 1 spatial-major scanning (Figure 4(a)) nor adding new temporal-major scanning Hydra blocks is effective for video data; we hypothesize that the former results in a weak temporal receptive field for the tokens, while the latter introduces excessive noise, hindering learning.

Through extensive experiments, we found a simple but surprisingly effective method – revising the scanning patterns of certain spatial-major scanning blocks to temporal-major scanning. As illustrated in Figure 3(b) and Figure 4(b), we directly change every two Hydra blocks with horizontal and vertical scans (H and V) to temporal-horizontal and temporal-vertical scans (TH and TV, *i.e.*, the SSMs scan all tokens at the same temporal position before moving to a horizontal or vertical adjacent token at the first frame), while having the other blocks to perform spatial-temporal frame-by-frame scanning (HT and VT). Note that for image data, temporal scans are absent, so all layers function as in stage 1. Therefore, this approach actually forces 40% of the Hydra blocks to learn additional temporal-major modeling.

4. Experiments

We provide the implementation details of our model, along with the results of text-to-image and text-to-video generation at different resolutions.

Implementation Details As mentioned in §3.2, our HTH model comprises 33 blocks, with every 10 Hydra blocks followed by a self-attention block. The model uses a hidden dimension of 3072 throughout, with Hydra configured to have an internal state dimension of 256, `ngroups` set to 1, a head dimension of 64, an expansion factor of $2\times$, and a convolution window size of 7. For both cross-attention and self-attention layers, the KV-dimension matches the model dimension (3072), utilizing 32 attention heads and incorporating RMSNorm (Zhang & Sennrich, 2019) for QK-Normalization (Henry et al., 2020). The MLP in each block applies an expansion ratio of $2\times$ and consists of two nonlinear layers. Together, the above configurations result in the final 5B-parameter HTH model. As illustrated in Figure 3, residual connections are employed at the layer level, linking features preceding each LayerNorm (Lei Ba et al., 2016) to the output features of the subsequent layer. We use a patch size of 2×2 to further compress the spatial dimension of latents produced by the VAE. To incorporate positional information, we use a non-learnable absolute sinusoidal positional embedding (Vaswani et al., 2017), which is directly added to the input tokens.

Training We adopt a multi-stage training strategy to enable high-resolution image and video generation. Initially, we train a base T2I model on 256p internal data for 200K iterations with a batch size of 1024, followed by an additional 286K iterations with an increased batch size of 3072. The starting learning rate is set to $1e-4$ and decays according to a cosine annealing schedule. Next,

- **1K T2I.** We apply a fast adaptation training to extend the model for high-resolution image generation. Specifically, we fine-tune the 256p base model on 1K-resolution images using a batch size of 576, training for only 10,000 iterations with a learning rate that rapidly decays from $5e-5$ to $1e-6$.

- **180p T2V.** To obtain a base video generation model, we continue training the T2I base model on a mixture of 256p images and 180p videos (characterized by a smaller number of frames on average and varying FPS) over 154K iterations. We adopt a stepwise learning rate reset approach, where the starting learning rate of the cosine annealing schedule is reset whenever the validation loss plateaus. In our experiment, the learning rate is reset four times: from $1e-4$ to $5e-5$, then to $3e-5$, and finally to $1e-5$. This training stage enables the model to synthesize video data while preserving the learned semantics and visual quality.
- **360p T2V.** Finally, we tune the 180p video model using 360p 128-frame video data with a batch size of 288. Leveraging a similar fast adaptation training strategy, we train the model for only 10K iterations with a learning rate that decays from $1e-5$ to $1e-6$.

We apply the diffusion noise scheduling and loss introduced in InstaFlow (Liu et al., 2023) and train the model following standard diffusion model training procedure (Ho et al., 2020) with classifier-free guidance (Ho & Salimans, 2022).

Inference At inference, we apply DDIM (Song et al., 2020) to denoise the latent representations. The denoised latents are then decoded by our internal VAE, with the resulting outputs presented and evaluated in this paper without any post-processing, such as super-resolution.

4.1. Results and Discussions

4.1.1. VISUALIZATION

We present several 1K+ images and 360p video frames generated by our HTH model in Figure 1 and Figure 2, respectively. Additional results, including playable videos, are provided in Appendix B.3 and the supplemental materials. The visualizations demonstrate that the model can produce high-fidelity outputs across diverse styles consistent with the given text prompts. Notably, for high-res image generation, despite being trained on mixed-aspect ratios 1K data (with extreme `Height:Width` ratios of 512:2048 and 2048:512), the model is capable of zero-shot generating around $3.5\times$ larger 2K images, including resolutions up to 1920×1920 , 1440×2560 , and 2560×1440 . We refer readers to Appendix B.2 for more details about the zero-shot experiments.

4.1.2. BENCHMARK EVALUATION

We compare our generated images and videos with existing approaches on the widely applied benchmarks. Specifically, we evaluate 256×256 images produced by our base image model on MSCOCO-30K (Lin et al., 2014), 1024×1024

Table 1. Comparison of 256×256 T2I generation.

Models	MSCOCO-30K
	FID↓
LDM (Rombach et al., 2022)	12.63
DALL-E 2 (Ramesh et al., 2022)	10.39
Imagen (Saharia et al., 2022)	7.27
eDiff-I (Balaji et al., 2022)	6.95
Transfusion (Zhou et al., 2024)	6.78
DeepFloyd (Stability AI, 2024)	6.66
RAPHAEL (Xue et al., 2024)	6.61
DiT (Ours, baseline)	12.53
HTH (Ours)	11.85

Table 2. Comparison of 1024×1024 T2I generation.

Models	MJHQ-30K		GenEval
	FID↓	CLIP-Score↑	Overall↑
SDXL (Podell et al., 2023)	8.76	28.60	0.55
PixArt- Σ (Chen et al., 2024a)	6.34	27.62	0.54
Playground v2.5 (Li et al., 2024a)	6.84	29.39	0.56
SD3-medium (Esser et al., 2024)	11.92	27.83	0.62
DALL-E 3 (OpenAI, 2023)	–	–	0.67
FLUX-dev (Black Forest Labs, 2024)	10.15	27.47	0.67
FLUX-schnell (Black Forest Labs, 2024)	7.94	28.14	0.71
DiT (Ours, baseline)	6.90	27.37	0.63
HTH (Ours)	6.52	27.26	0.58

images produced by our 1K-tuned image model on MJHQ-30K (Li et al., 2024a) and GenEval (Ghosh et al., 2024), as well as the videos produced by our 180p and 360p T2V models on VBench (Huang et al., 2024), respectively. Our model follows the standard guidelines when generating the results without tricks like prompt rewriting. All image models we compared with are diffusion-based models.

256×256 & 1024×1024 T2I. As shown in Table 1 and Table 2, we compare our generation results against a wide range of recent approaches. Our HTH model demonstrates strong performance, achieving results highly comparable to other state-of-the-art methods in terms of FID (Heusel et al., 2017) and CLIP-Score (Radford et al., 2021) when generating high-resolution images. Notably, our model, built on the DiT framework, surpasses DiT on both the MSCOCO and MJHQ benchmarks. However, our model underperforms on GenEval, an object-centric evaluation metric. Upon analyzing the evaluation dimensions and text-image pairs, we observe that compared to the DiT baseline, the SSM-based solution exhibits a higher failure rate in generating structure-coherent objects and more struggles with creating co-occurring objects that align with the text prompt (score 0.67 vs. 0.75). We hypothesize that this limitation stems from the inherent constraints of SSM-dense models, particularly their insufficient capacity to model long-range global dependencies effectively.

180p & 360p T2V. We compare our generated videos with ModelScope (Wang et al., 2023a), LaVie (Wang

Table 3. Comparison with existing text-to-video models on VBench (Huang et al., 2024). The exact resolutions of our 180p and 360p videos are 192×320 and 384×640 , respectively. We choose 12 evaluation dimensions. Higher metric values indicate better performance.

Models	Subject Consistency	Background Consistency	Aesthetic Quality	Object Class	Scene	Human Action	Apperance Style	Temporal Style	Temporal Flickering	Motion Smoothness	Dynamic Degree	Overall Consistency
ModelScope	89.87	95.29	56.39	82.25	39.26	92.40	23.39	25.37	98.28	95.79	66.39	25.67
LaVie	91.41	97.47	54.94	91.82	52.69	96.80	23.56	25.93	98.30	96.38	49.72	26.41
Show-1	95.53	98.02	57.35	93.07	47.03	95.60	23.06	25.28	99.12	98.24	44.44	27.46
OpenSora-v1.2	96.75	97.61	56.18	82.22	42.44	91.20	23.95	24.55	99.47	98.50	42.39	26.85
VideoCrafter-2.0	96.85	98.22	63.13	92.55	55.29	95.00	25.13	25.84	98.41	97.73	42.50	28.23
T2V-Turbo (VC2)	96.28	97.02	63.04	93.96	55.58	95.20	24.42	25.51	97.48	97.34	49.17	28.16
CogVideoX-5B	96.23	96.52	61.98	85.23	53.20	99.40	24.91	25.38	98.66	96.92	70.97	28.23
Pika	96.94	97.36	62.04	88.72	49.83	86.20	22.26	24.22	99.74	99.50	47.50	25.94
Kling (2024-07)	98.33	97.60	61.21	87.24	50.86	93.40	19.62	24.17	99.30	99.40	46.94	26.42
Gen3	97.10	96.62	63.34	87.81	54.57	96.40	24.31	25.33	98.61	99.23	60.14	26.69
ARLON	93.41	97.10	61.01	89.80	54.43	–	–	–	99.37	98.92	52.77	27.27
Emu3	95.32	97.69	59.64	86.17	37.11	77.71	20.92	23.26	98.57	98.93	79.27	24.79
HTH-180p (Ours)	95.71	98.53	55.58	91.61	50.12	97.60	25.03	25.34	98.92	98.87	79.72	27.36
HTH-360p (Ours)	91.36	95.34	62.71	86.08	46.28	96.80	25.09	25.10	97.00	98.75	84.44	27.41

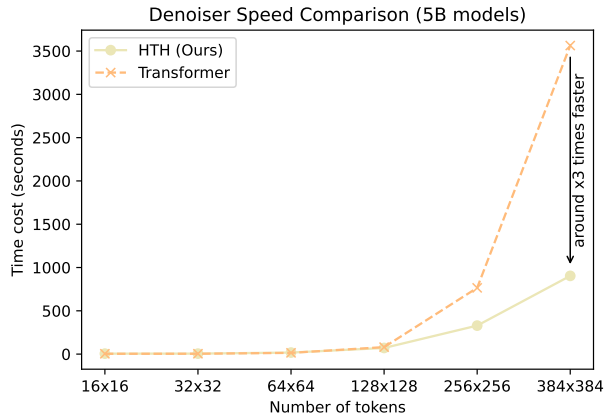


Figure 5. Denoiser inference speed comparison between HTH and Transformer (our DiT baseline).

et al., 2023b), Show-1 (Zhang et al., 2024a), OpenSora-v1.2 (Open-Sora, 2024), VideoCrafter-2.0 (Chen et al., 2023), T2V-Turbo (VC2) (Li et al., 2024b), CogVideoX-5B (Yang et al., 2024), Pika (Pika Labs, 2023), Kling (Kling AI, 2024), Gen3 (Runway, 2024), ARLON (Li et al., 2024c), and Emu3 (Wang et al., 2024c) on the VBench benchmark (Huang et al., 2024). Emu3 is the only autoregressive model on the list, while all other approaches are diffusion-based. Our HTH model demonstrates highly comparable performance to existing methods across all evaluation dimensions. In particular, the 360p model excels in *Aesthetic Quality*, as well as *Appearance* and *Temporal Style*. Additionally, it generates accurate and realistic *Human Actions* while producing videos with a significantly higher *Dynamic Degree* and a good *Overall Consistency*.

4.1.3. EFFICIENCY

In Figure 5, we compare the wall-time inference speed between a Transformer-based denoiser and our proposed HTH denoiser for processing varying numbers of tokens. Both

models have 5B parameters and execute 50 (denoising) steps, with all self-attention layers employing the Flash-Attention 2 implementation (Dao, 2023). At a token length of 128^2 , corresponding to the largest 2K images we tested with our HTH model, the speed difference is minor, with HTH being only 10 seconds faster. However, as the resolution increases, the performance gap widens exponentially. This observation is consistent with the quadratic computational complexity associated with global self-attention. A token length of 384^2 roughly corresponds to an 8K image or a 6-second 1K video at 24 FPS under our $\times 8$ spatial and $\frac{16}{5} \times$ temporal compression rates and a patch size of 2; this suggests that the efficiency benefits of the SSM-based model become more pronounced for very long visual sequences. The current implementation of bidirectional SSMs, like Hydra, presents significant potential for hardware (CUDA) optimization, including kernel operation integration. We intend to pursue these optimizations in future work.

5. Conclusion

In this paper, we propose the Hydra-Transformer Hybrid (HTH) diffusion model, a large-scale framework designed to push the boundaries of applying state space models (SSMs) to high-resolution image and long video generation. Our experiments show that using simple scanning strategies, models built with sequential and subquadratic token mixers, such as bidirectional SSMs, can achieve performance comparable to Transformer-based models while demonstrating superior inference efficiency and the potential to zero-shot higher-resolution images. We identify essential limitations and future directions of SSM-based generative models and share them in Appendix A. We hope our findings will provide valuable insights and inspire future research on leveraging state space models and broader, more efficient sub-quadratic complexity architectures to tackle complex visual generation problems.

References

- Balaji, Y., Nah, S., Huang, X., Vahdat, A., Song, J., Zhang, Q., Kreis, K., Aittala, M., Aila, T., Laine, S., et al. ediff-i: Text-to-image diffusion models with an ensemble of expert denoisers. *arXiv preprint arXiv:2211.01324*, 2022.
- Bar-Tal, O., Chefer, H., Tov, O., Herrmann, C., Paiss, R., Zada, S., Ephrat, A., Hur, J., Li, Y., Michaeli, T., et al. Lumiere: A space-time diffusion model for video generation. *arXiv preprint arXiv:2401.12945*, 2024.
- Beltagy, I., Peters, M. E., and Cohan, A. Longformer: The long-document transformer. *arXiv preprint arXiv:2004.05150*, 2020.
- Bick, A., Li, K. Y., Xing, E. P., Kolter, J. Z., and Gu, A. Transformers to ssms: Distilling quadratic knowledge to subquadratic models. *arXiv preprint arXiv:2408.10189*, 2024.
- Black Forest Labs. Flux by black forest labs, 2024. URL <https://github.com/black-forest-labs/flux>.
- Blattmann, A., Rombach, R., Ling, H., Dockhorn, T., Kim, S. W., Fidler, S., and Kreis, K. Align your latents: High-resolution video synthesis with latent diffusion models. In *Proceedings of the IEEE/CVF Conference on Computer Vision and Pattern Recognition*, pp. 22563–22575, 2023.
- Botev, A., De, S., Smith, S. L., Fernando, A., Muraru, G.-C., Haroun, R., Berrada, L., Pascanu, R., Sessa, P. G., Dadashi, R., et al. Recurrentgemma: Moving past transformers for efficient open language models. *arXiv preprint arXiv:2404.07839*, 2024.
- Chang, H., Zhang, H., Barber, J., Maschinot, A., Lezama, J., Jiang, L., Yang, M.-H., Murphy, K., Freeman, W. T., Rubinstein, M., Li, Y., and Krishnan, D. Muse: Text-to-image generation via masked generative transformers. *arXiv preprint arXiv:2301.00704*, 2023.
- Cheang, C.-L., Chen, G., Jing, Y., Kong, T., Li, H., Li, Y., Liu, Y., Wu, H., Xu, J., Yang, Y., et al. Gr-2: A generative video-language-action model with web-scale knowledge for robot manipulation. *arXiv preprint arXiv:2410.06158*, 2024.
- Chen, H., Xia, M., He, Y., Zhang, Y., Cun, X., Yang, S., Xing, J., Liu, Y., Chen, Q., Wang, X., et al. Videocrafter1: Open diffusion models for high-quality video generation. *arXiv preprint arXiv:2310.19512*, 2023.
- Chen, J., Ge, C., Xie, E., Wu, Y., Yao, L., Ren, X., Wang, Z., Luo, P., Lu, H., and Li, Z. Pixart- σ : Weak-to-strong training of diffusion transformer for 4k text-to-image generation. *arXiv preprint arXiv:2403.04692*, 2024a.
- Chen, W., Niu, L., Lu, Z., Meng, F., and Zhou, J. Maskmamba: A hybrid mamba-transformer model for masked image generation. *arXiv preprint arXiv:2409.19937*, 2024b.
- Choromanski, K., Likhoshesterov, V., Dohan, D., Song, X., Gane, A., Sarlos, T., Hawkins, P., Davis, J., Mohiuddin, A., Kaiser, L., et al. Rethinking attention with performers. *arXiv preprint arXiv:2009.14794*, 2020.
- Chung, H. W., Hou, L., Longpre, S., Zoph, B., Tay, Y., Fedus, W., Li, Y., Wang, X., Dehghani, M., Brahma, S., et al. Scaling instruction-finetuned language models. *Journal of Machine Learning Research*, 25(70):1–53, 2024.
- Dao, T. Flashattention-2: Faster attention with better parallelism and work partitioning. *arXiv preprint arXiv:2307.08691*, 2023.
- Dao, T. and Gu, A. Transformers are ssms: Generalized models and efficient algorithms through structured state space duality. *arXiv preprint arXiv:2405.21060*, 2024.
- De, S., Smith, S. L., Fernando, A., Botev, A., Cristian-Muraru, G., Gu, A., Haroun, R., Berrada, L., Chen, Y., Srinivasan, S., et al. Griffin: Mixing gated linear recurrences with local attention for efficient language models. *arXiv preprint arXiv:2402.19427*, 2024.
- Dehghani, M., Djolonga, J., Mustafa, B., Padlewski, P., Heek, J., Gilmer, J., Steiner, A. P., Caron, M., Geirhos, R., Alabdulmohsin, I., et al. Scaling vision transformers to 22 billion parameters. In *International Conference on Machine Learning*, pp. 7480–7512. PMLR, 2023.
- Dhariwal, P. and Nichol, A. Diffusion models beat gans on image synthesis. *Advances in neural information processing systems*, 34:8780–8794, 2021.
- Dosovitskiy, A. An image is worth 16x16 words: Transformers for image recognition at scale. *arXiv preprint arXiv:2010.11929*, 2020.
- Du, Y., Yang, S., Dai, B., Dai, H., Nachum, O., Tenenbaum, J., Schuurmans, D., and Abbeel, P. Learning universal policies via text-guided video generation. *Advances in Neural Information Processing Systems*, 36, 2024.
- Esser, P., Rombach, R., and Ommer, B. Taming transformers for high-resolution image synthesis. In *Proceedings of the IEEE/CVF conference on computer vision and pattern recognition*, pp. 12873–12883, 2021.
- Esser, P., Kulal, S., Blattmann, A., Entezari, R., Müller, J., Saini, H., Levi, Y., Lorenz, D., Sauer, A., Boesel, F., et al. Scaling rectified flow transformers for high-resolution image synthesis. In *Forty-first International Conference on Machine Learning*, 2024.

- Fei, Z., Fan, M., Yu, C., Li, D., Zhang, Y., and Huang, J. Dimba: Transformer-mamba diffusion models. *arXiv preprint arXiv:2406.01159*, 2024.
- Gao, Y., Huang, J., Sun, X., Jie, Z., Zhong, Y., and Ma, L. Matten: Video generation with mamba-attention. *arXiv preprint arXiv:2405.03025*, 2024.
- Ghosh, D., Hajishirzi, H., and Schmidt, L. Geneval: An object-focused framework for evaluating text-to-image alignment. *Advances in Neural Information Processing Systems*, 36, 2024.
- Girdhar, R., Singh, M., Brown, A., Duval, Q., Azadi, S., Rambhatla, S. S., Shah, A., Yin, X., Parikh, D., and Misra, I. Emu video: Factorizing text-to-video generation by explicit image conditioning. *arXiv preprint arXiv:2311.10709*, 2023.
- Gu, A. and Dao, T. Mamba: Linear-time sequence modeling with selective state spaces. *arXiv preprint arXiv:2312.00752*, 2023.
- Henry, A., Dachapally, P. R., Pawar, S., and Chen, Y. Query-key normalization for transformers. *arXiv preprint arXiv:2010.04245*, 2020.
- Heusel, M., Ramsauer, H., Unterthiner, T., Nessler, B., and Hochreiter, S. Gans trained by a two time-scale update rule converge to a local nash equilibrium. *Advances in neural information processing systems*, 30, 2017.
- Ho, J. and Salimans, T. Classifier-free diffusion guidance. *arXiv preprint arXiv:2207.12598*, 2022.
- Ho, J., Jain, A., and Abbeel, P. Denoising diffusion probabilistic models. *Advances in neural information processing systems*, 33:6840–6851, 2020.
- Ho, J., Chan, W., Saharia, C., Whang, J., Gao, R., Gritsenko, A., Kingma, D. P., Poole, B., Norouzi, M., Fleet, D. J., and Salimans, T. Imagen video: High definition video generation with diffusion models. *arXiv preprint arXiv:2210.02303*, 2022.
- Hong, W., Ding, M., Zheng, W., Liu, X., and Tang, J. Cogvideo: Large-scale pretraining for text-to-video generation via transformers. *arXiv preprint arXiv:2205.15868*, 2022.
- Hong, Y., Zhang, K., Gu, J., Bi, S., Zhou, Y., Liu, D., Liu, F., Sunkavalli, K., Bui, T., and Tan, H. Lrm: Large reconstruction model for single image to 3d. *arXiv preprint arXiv:2311.04400*, 2023.
- Hu, V. T., Baumann, S. A., Gui, M., Grebenkova, O., Ma, P., Fischer, J., and Ommer, B. Zigma: A dit-style zigzag mamba diffusion model. *arXiv preprint arXiv:2403.13802*, 2024.
- Huang, Z., He, Y., Yu, J., Zhang, F., Si, C., Jiang, Y., Zhang, Y., Wu, T., Jin, Q., Chanpaisit, N., et al. Vbench: Comprehensive benchmark suite for video generative models. In *Proceedings of the IEEE/CVF Conference on Computer Vision and Pattern Recognition*, pp. 21807–21818, 2024.
- Hwang, S., Lahoti, A., Dao, T., and Gu, A. Hydra: Bidirectional state space models through generalized matrix mixers. *arXiv preprint arXiv:2407.09941*, 2024.
- Jelassi, S., Brandfonbrener, D., Kakade, S. M., and Malach, E. Repeat after me: Transformers are better than state space models at copying. *arXiv preprint arXiv:2402.01032*, 2024.
- Katharopoulos, A., Vyas, A., Pappas, N., and Fleuret, F. Transformers are rnns: Fast autoregressive transformers with linear attention. In *International conference on machine learning*, pp. 5156–5165. PMLR, 2020.
- Kitaev, N., Kaiser, Ł., and Levskaya, A. Reformer: The efficient transformer. *arXiv preprint arXiv:2001.04451*, 2020.
- Kling AI. Kling, 2024. URL <https://klingai.com/>.
- Kondratyuk, D., Yu, L., Gu, X., Lezama, J., Huang, J., Schindler, G., Hornung, R., Birodkar, V., Yan, J., Chiu, M.-C., et al. Videopoet: A large language model for zero-shot video generation. *arXiv preprint arXiv:2312.14125*, 2023.
- Lei Ba, J., Kiros, J. R., and Hinton, G. E. Layer normalization. *ArXiv e-prints*, pp. arXiv–1607, 2016.
- Li, D., Kamko, A., Akhgari, E., Sabet, A., Xu, L., and Doshi, S. Playground v2. 5: Three insights towards enhancing aesthetic quality in text-to-image generation. *arXiv preprint arXiv:2402.17245*, 2024a.
- Li, J., Feng, W., Fu, T.-J., Wang, X., Basu, S., Chen, W., and Wang, W. Y. T2v-turbo: Breaking the quality bottleneck of video consistency model with mixed reward feedback. *arXiv preprint arXiv:2405.18750*, 2024b.
- Li, S., Li, C., Zhu, W., Yu, B., Zhao, Y., Wan, C., You, H., Shi, H., and Lin, Y. Instant-3d: Instant neural radiance field training towards on-device ar/vr 3d reconstruction. In *Proceedings of the 50th Annual International Symposium on Computer Architecture*, pp. 1–13, 2023.
- Li, Z., Hu, S., Liu, S., Zhou, L., Choi, J., Meng, L., Guo, X., Li, J., Ling, H., and Wei, F. Arlon: Boosting diffusion transformers with autoregressive models for long video generation. *arXiv preprint arXiv:2410.20502*, 2024c.
- Lieber, O., Lenz, B., Bata, H., Cohen, G., Osin, J., Dalmedigos, I., Safahi, E., Meirom, S., Belinkov, Y., Shalev-Shwartz, S., et al. Jamba: A hybrid transformer-mamba language model. *arXiv preprint arXiv:2403.19887*, 2024.

- Lin, T.-Y., Maire, M., Belongie, S., Hays, J., Perona, P., Ramanan, D., Dollár, P., and Zitnick, C. L. Microsoft coco: Common objects in context. In *Computer Vision–ECCV 2014: 13th European Conference, Zurich, Switzerland, September 6–12, 2014, Proceedings, Part V 13*, pp. 740–755. Springer, 2014.
- Liu, S., Yu, W., Tan, Z., and Wang, X. Linfusion: 1 gpu, 1 minute, 16k image. *arXiv preprint arXiv:2409.02097*, 2024.
- Liu, X., Zhang, X., Ma, J., Peng, J., et al. Instaflo: One step is enough for high-quality diffusion-based text-to-image generation. In *The Twelfth International Conference on Learning Representations*, 2023.
- Merrill, W., Petty, J., and Sabharwal, A. The illusion of state in state-space models. *arXiv preprint arXiv:2404.08819*, 2024.
- Open-Sora. Open-sora 1.2 report, 2024. URL <https://github.com/hpcaitech/Open-Sora>.
- OpenAI. Dall-e 3 by openai, 2023. URL <https://openai.com/dall-e-3>.
- Peebles, W. and Xie, S. Scalable diffusion models with transformers. In *Proceedings of the IEEE/CVF International Conference on Computer Vision*, pp. 4195–4205, 2023.
- Peng, B., Alcaide, E., Anthony, Q., Albalak, A., Arcadinho, S., Biderman, S., Cao, H., Cheng, X., Chung, M., Grella, M., et al. Rwkv: Reinventing rnns for the transformer era. *arXiv preprint arXiv:2305.13048*, 2023.
- Pika Labs. Pika, 2023. URL <https://github.com/hpcaitech/Open-Sora>.
- Podell, D., English, Z., Lacey, K., Blattmann, A., Dockhorn, T., Müller, J., Penna, J., and Rombach, R. Sdxl: Improving latent diffusion models for high-resolution image synthesis. *arXiv preprint arXiv:2307.01952*, 2023.
- Qin, Z., Sun, W., Deng, H., Li, D., Wei, Y., Lv, B., Yan, J., Kong, L., and Zhong, Y. cosformer: Rethinking softmax in attention. *arXiv preprint arXiv:2202.08791*, 2022.
- Radford, A., Kim, J. W., Hallacy, C., Ramesh, A., Goh, G., Agarwal, S., Sastry, G., Askell, A., Mishkin, P., Clark, J., et al. Learning transferable visual models from natural language supervision. In *International conference on machine learning*, pp. 8748–8763. PMLR, 2021.
- Raffel, C., Shazeer, N., Roberts, A., Lee, K., Narang, S., Matena, M., Zhou, Y., Li, W., and Liu, P. J. Exploring the limits of transfer learning with a unified text-to-text transformer. *Journal of machine learning research*, 21 (140):1–67, 2020.
- Ramesh, A., Dhariwal, P., Nichol, A., Chu, C., and Chen, M. Hierarchical text-conditional image generation with clip latents. *arXiv preprint arXiv:2204.06125*, 1(2):3, 2022.
- Rombach, R., Blattmann, A., Lorenz, D., Esser, P., and Ommer, B. High-resolution image synthesis with latent diffusion models. In *Proceedings of the IEEE/CVF conference on computer vision and pattern recognition*, pp. 10684–10695, 2022.
- Ruiz, N., Li, Y., Jampani, V., Pritch, Y., Rubinstein, M., and Aberman, K. Dreambooth: Fine tuning text-to-image diffusion models for subject-driven generation. In *Proceedings of the IEEE/CVF conference on computer vision and pattern recognition*, pp. 22500–22510, 2023.
- Runway. Introducing gen-3 alpha: A new frontier for video generation, 2024. URL <https://runwayml.com/research/introducing-gen-3-alpha>.
- Saharia, C., Chan, W., Saxena, S., Li, L., Whang, J., Denton, E., Ghasemipour, S. K. S., Ayan, B. K., Mahdavi, S. S., Lopes, R. G., Salimans, T., Ho, J., Fleet, D. J., and Norouzi, M. Photorealistic text-to-image diffusion models with deep language understanding. *arXiv preprint arXiv:2205.11487*, 2022.
- Shen, Z., Zhang, M., Zhao, H., Yi, S., and Li, H. Efficient attention: Attention with linear complexities. In *Proceedings of the IEEE/CVF winter conference on applications of computer vision*, pp. 3531–3539, 2021.
- Shi, Y., Dong, M., Li, M., and Xu, C. Vssd: Vision mamba with non-causal state space duality. *arXiv preprint arXiv:2407.18559*, 2024.
- Song, J., Meng, C., and Ermon, S. Denoising diffusion implicit models. *arXiv preprint arXiv:2010.02502*, 2020.
- Stability AI. If by deepfloyd lab at stability ai, 2024. URL <https://stability.ai/news/deepfloyd-if-text-to-image-model>.
- Su, J., Ahmed, M., Lu, Y., Pan, S., Bo, W., and Liu, Y. Roformer: Enhanced transformer with rotary position embedding. *Neurocomputing*, 568:127063, 2024.
- Sun, P., Jiang, Y., Chen, S., Zhang, S., Peng, B., Luo, P., and Yuan, Z. Autoregressive model beats diffusion: Llama for scalable image generation. *arXiv preprint arXiv:2406.06525*, 2024.
- Sun, Y., Dong, L., Huang, S., Ma, S., Xia, Y., Xue, J., Wang, J., and Wei, F. Retentive network: A successor to transformer for large language models. *arXiv preprint arXiv:2307.08621*, 2023.

- Vaswani, A., Shazeer, N., Parmar, N., Uszkoreit, J., Jones, L., Gomez, A. N., Kaiser, L., and Polosukhin, I. Attention is all you need. *Advances in Neural Information Processing Systems*, 2017.
- Waleffe, R., Byeon, W., Riach, D., Norick, B., Korthikanti, V., Dao, T., Gu, A., Hatamizadeh, A., Singh, S., Narayanan, D., et al. An empirical study of mamba-based language models. *arXiv preprint arXiv:2406.07887*, 2024.
- Wang, J., Yuan, H., Chen, D., Zhang, Y., Wang, X., and Zhang, S. Modelscope text-to-video technical report. *arXiv preprint arXiv:2308.06571*, 2023a.
- Wang, J., Paliotta, D., May, A., Rush, A. M., and Dao, T. The mamba in the llama: Distilling and accelerating hybrid models. *arXiv preprint arXiv:2408.15237*, 2024a.
- Wang, S., Li, B. Z., Khabsa, M., Fang, H., and Ma, H. Linformer: Self-attention with linear complexity. *arXiv preprint arXiv:2006.04768*, 2020.
- Wang, S., Leroy, V., Cabon, Y., Chidlovskii, B., and Revaud, J. Dust3r: Geometric 3d vision made easy. In *Proceedings of the IEEE/CVF Conference on Computer Vision and Pattern Recognition*, pp. 20697–20709, 2024b.
- Wang, X., Zhang, X., Luo, Z., Sun, Q., Cui, Y., Wang, J., Zhang, F., Wang, Y., Li, Z., Yu, Q., et al. Emu3: Next-token prediction is all you need. *arXiv preprint arXiv:2409.18869*, 2024c.
- Wang, Y., Chen, X., Ma, X., Zhou, S., Huang, Z., Wang, Y., Yang, C., He, Y., Yu, J., Yang, P., et al. Lavie: High-quality video generation with cascaded latent diffusion models. *arXiv preprint arXiv:2309.15103*, 2023b.
- Watson, D., Saxena, S., Li, L., Tagliasacchi, A., and Fleet, D. J. Controlling space and time with diffusion models. *arXiv preprint arXiv:2407.07860*, 2024.
- Wu, H., Jing, Y., Cheang, C., Chen, G., Xu, J., Li, X., Liu, M., Li, H., and Kong, T. Unleashing large-scale video generative pre-training for visual robot manipulation. *arXiv preprint arXiv:2312.13139*, 2023.
- Xie, E., Chen, J., Chen, J., Cai, H., Tang, H., Lin, Y., Zhang, Z., Li, M., Zhu, L., Lu, Y., and Han, S. Sana: Efficient high-resolution image synthesis with linear diffusion transformers. *arXiv preprint arXiv:2410.10629*, 2024.
- Xiong, R., Yang, Y., He, D., Zheng, K., Zheng, S., Xing, C., Zhang, H., Lan, Y., Wang, L., and Liu, T. On layer normalization in the transformer architecture. In *International Conference on Machine Learning*, pp. 10524–10533. PMLR, 2020.
- Xu, R., Yang, S., Wang, Y., Du, B., and Chen, H. A survey on vision mamba: Models, applications and challenges. *arXiv preprint arXiv:2404.18861*, 2024.
- Xu, Y., Tan, H., Luan, F., Bi, S., Wang, P., Li, J., Shi, Z., Sunkavalli, K., Wetzstein, G., Xu, Z., et al. Dmv3d: Denoising multi-view diffusion using 3d large reconstruction model. *arXiv preprint arXiv:2311.09217*, 2023.
- Xue, Z., Song, G., Guo, Q., Liu, B., Zong, Z., Liu, Y., and Luo, P. Raphael: Text-to-image generation via large mixture of diffusion paths. *Advances in Neural Information Processing Systems*, 36, 2024.
- Yan, J. N., Gu, J., and Rush, A. M. Diffusion models without attention. *arXiv preprint arXiv:2311.18257*, 2023.
- Yan, W., Zhang, Y., Abbeel, P., and Srinivas, A. Videogpt: Video generation using vq-vae and transformers. *arXiv preprint arXiv:2104.10157*, 2021.
- Yang, M., Du, Y., Ghasemipour, K., Tompson, J., Schuurmans, D., and Abbeel, P. Learning interactive real-world simulators. *arXiv preprint arXiv:2310.06114*, 2023a.
- Yang, S., Wang, B., Shen, Y., Panda, R., and Kim, Y. Gated linear attention transformers with hardware-efficient training. *arXiv preprint arXiv:2312.06635*, 2023b.
- Yang, Z., Teng, J., Zheng, W., Ding, M., Huang, S., Xu, J., Yang, Y., Hong, W., Zhang, X., Feng, G., et al. Cogvideox: Text-to-video diffusion models with an expert transformer. *arXiv preprint arXiv:2408.06072*, 2024.
- Yi, X., Wu, Z., Shen, Q., Xu, Q., Zhou, P., Lim, J.-H., Yan, S., Wang, X., and Zhang, H. Mvgamba: Unify 3d content generation as state space sequence modeling. *arXiv preprint arXiv:2406.06367*, 2024.
- Yu, L., Lezama, J., Gundavarapu, N. B., Versari, L., Sohn, K., Minnen, D., Cheng, Y., Birodkar, V., Gupta, A., Gu, X., et al. Language model beats diffusion—tokenizer is key to visual generation. *arXiv preprint arXiv:2310.05737*, 2023.
- Zhang, B. and Sennrich, R. Root mean square layer normalization. *Advances in Neural Information Processing Systems*, 32, 2019.
- Zhang, D. J., Wu, J. Z., Liu, J.-W., Zhao, R., Ran, L., Gu, Y., Gao, D., and Shou, M. Z. Show-1: Marrying pixel and latent diffusion models for text-to-video generation. *International Journal of Computer Vision*, pp. 1–15, 2024a.
- Zhang, H., Zhu, Y., Wang, D., Zhang, L., Chen, T., Wang, Z., and Ye, Z. A survey on visual mamba. *Applied Sciences*, 14(13):5683, 2024b.

Zhang, Z., Liu, A., Reid, I., Hartley, R., Zhuang, B., and Tang, H. Motion mamba: Efficient and long sequence motion generation with hierarchical and bidirectional selective ssm. *arXiv e-prints*, pp. arXiv–2403, 2024c.

Zhou, C., Yu, L., Babu, A., Tirumala, K., Yasunaga, M., Shamis, L., Kahn, J., Ma, X., Zettlemoyer, L., and Levy, O. Transfusion: Predict the next token and diffuse images with one multi-modal model. *arXiv preprint arXiv:2408.11039*, 2024.

Zhu, L., Huang, Z., Liao, B., Liew, J. H., Yan, H., Feng, J., and Wang, X. Dig: Scalable and efficient diffusion models with gated linear attention. *arXiv preprint arXiv:2405.18428*, 2024.

Ziwen, C., Tan, H., Zhang, K., Bi, S., Luan, F., Hong, Y., Fuxin, L., and Xu, Z. Long-lrm: Long-sequence large reconstruction model for wide-coverage gaussian splats. *arXiv preprint arXiv:2410.12781*, 2024.

Zuo, S., Liu, X., Jiao, J., Charles, D., Manavoglu, E., Zhao, T., and Gao, J. Efficient long sequence modeling via state space augmented transformer. *arXiv preprint arXiv:2212.08136*, 2022.

A. Limitations and Future Directions

Due to the extensive scope of this work and constraints in computational resources, we identify and share several limitations of our system that we believe are valuable for future research:

- **SSM-friendly pipeline.** Our model is built upon the existing DiT (Peebles & Xie, 2023) pipeline, which is specifically tailored and optimized for Transformer-based models and global attention operations. However, certain critical components, such as positional encoding, may be suboptimal for informing SSMs about spatial continuity. Improving these aspects is essential to better align the pipeline with SSM-based architectures.
- **Conditioning mechanisms.** The sequential nature of SSMs imposes constraints on how conditions are introduced to latent representations. In this work, we employ simple cross-attention to incorporate textual conditions, but the results generally exhibit inferior semantic understanding (*e.g.*, worse entity composition and structural coherence) compared to Transformer-based models. Developing more effective conditioning mechanisms for SSMs is a promising direction for future exploration.
- **SSM optimization.** The formulation and hardware optimization of SSMs remain at an early stage. Further research is needed to design SSMs better suited for processing N-dimensional visual data while maintaining high computational efficiency.

B. Additional Results

B.1. Comparison of Token Mixers

As shown in our small-scale experiment (Figure 6), we compared the generation quality across unidirectional SSM, bidirectional SSM, the state-sharing VSSD (Shi et al., 2024), self-attention, and Hydra. We constructed 1B-parameter models with the different token mixers above while keeping all other components identical and trained each model for 300K iterations. Hydra demonstrated clearly superior visual quality than the other SSM-based models, particularly in structural coherence and correctness, while achieving better semantic alignment with the text prompt. Its performance is also highly comparable to the model employing self-attention.

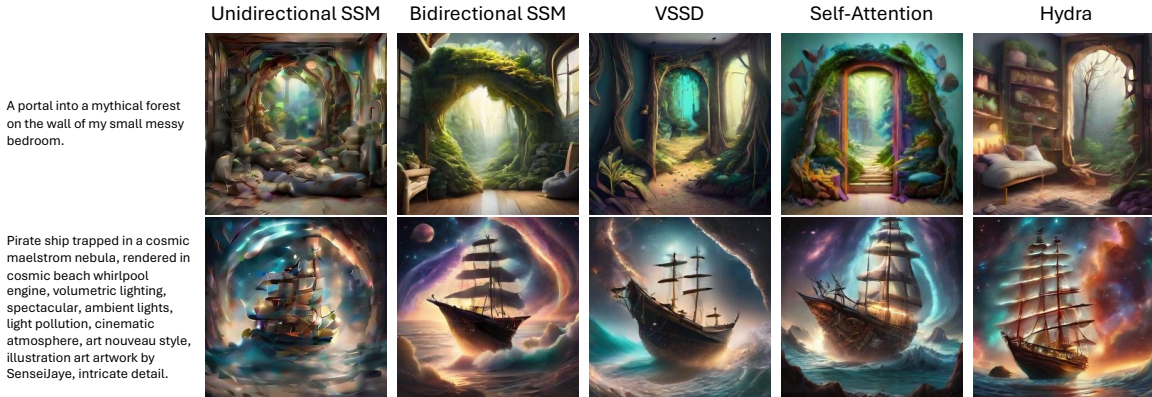


Figure 6. Example 256×256 -resolution T2I generation results of different token mixers. SSMs and Hydra models are based on Mamba-2 (Dao & Gu, 2024). The Bidirectional SSM and Hydra apply interleaved horizontal and vertical raster scans across model blocks. None of the models in this small-scale experiment is hybrid (*i.e.*, all blocks use the same token mixer).

B.2. Higher-Res Zero-shot Generation

We further compare the zero-shot performance of our SSM-dominant architecture with pure Transformer models, as shown in Figure 7. All models are of the same scale and are trained exclusively on 256p images, but are tasked with generating 512p images. The Transformer-based model with absolute positional embedding (APE) (Vaswani et al., 2017) struggles to generalize to higher resolutions, resulting in severe checkerboard artifacts. While models using relative positional encoding, such as RoPE (Su et al., 2024), achieve better results, noticeable inconsistency and noise persist. In contrast, our proposed

HTH model naturally generalizes to synthesize $\times 4$ times larger images, benefiting from the strong locality properties inherent to the state space model.

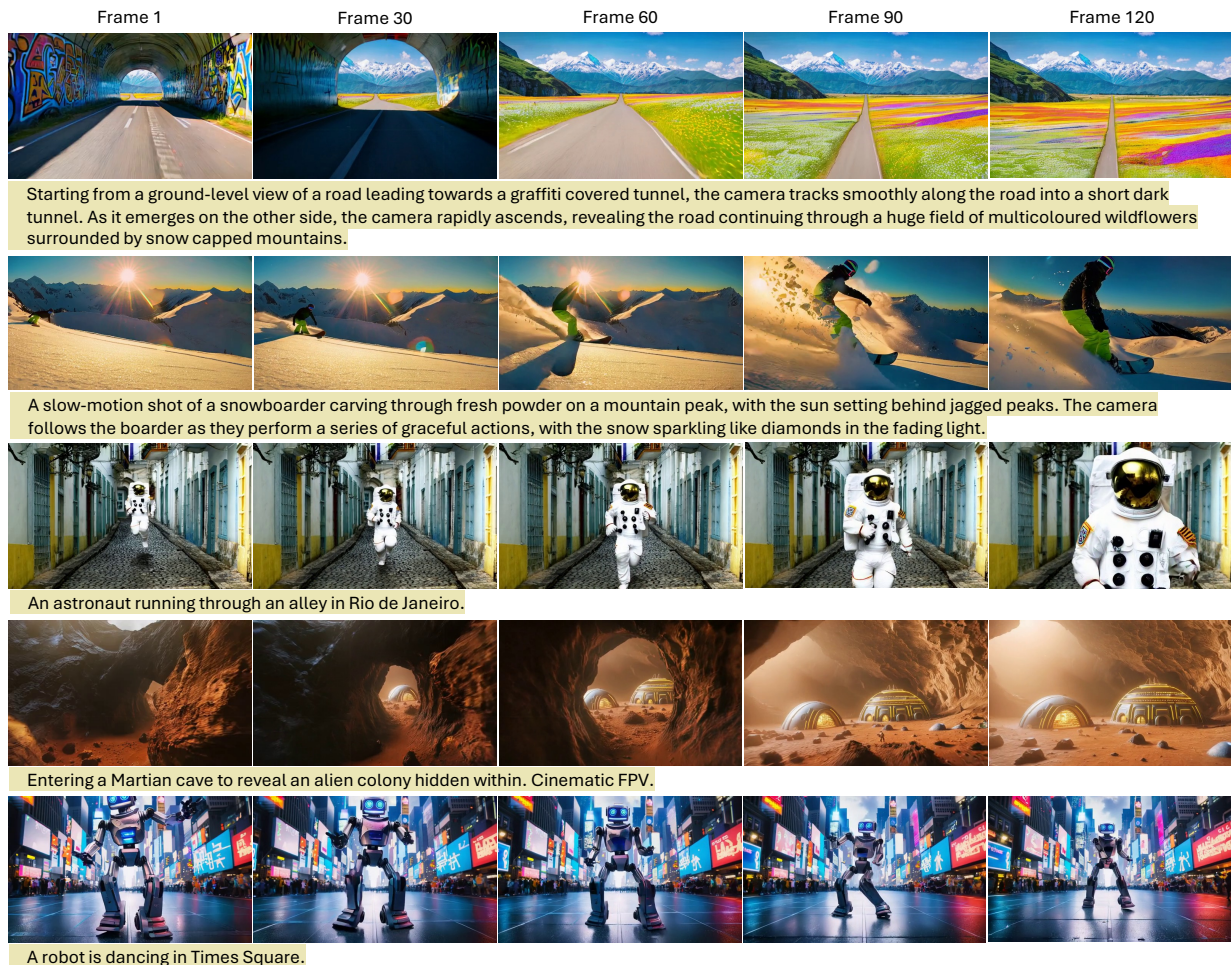


An astronaut running through an alley in Rio de Janeiro.

Figure 7. Zero-shot comparison at higher resolution. We compare our HTH model with the same-scale Transformer-based models (SA: Self-Attention) with Absolute Positional Embedding (APE) or Rotary Positional Embedding (RoPE). All models are trained on 256p image data and evaluated on 416 \times 608 images in a zero-shot manner.

B.3. Visualization

The following pages provide additional visualization of generated images in various aspect ratios up to 2560 \times 2560 resolution, and some extracted frames from generated 360p 128-frame videos. Please also refer to the Supplementary Materials for more playable videos.



Starting from a ground-level view of a road leading towards a graffiti covered tunnel, the camera tracks smoothly along the road into a short dark tunnel. As it emerges on the other side, the camera rapidly ascends, revealing the road continuing through a huge field of multicoloured wildflowers surrounded by snow capped mountains.

A slow-motion shot of a snowboarder carving through fresh powder on a mountain peak, with the sun setting behind jagged peaks. The camera follows the boarder as they perform a series of graceful actions, with the snow sparkling like diamonds in the fading light.

An astronaut running through an alley in Rio de Janeiro.

Entering a Martian cave to reveal an alien colony hidden within. Cinematic FPV.

A robot is dancing in Times Square.

Figure 8. Text-to-360p 128 frames video generation results produced by our Hydra-Transformer Hybrid model. Please zoom in for a clearer visualization.

Pushing the Boundaries of State Space Models for Image and Video Generation



Art collection style and fashion shoot, in the style of made of glass, dark blue and light pink, paul rand, solarpunk, camille vivier, beth didonato hair, barbiecore, hyper-realistic.



Flat drawing illustration, flat drawing, illustration, girl in pajamas sitting on the bed, a puppy, sunset, the light of the setting sun enters the house through the window, detailed light and shadow, high detail, 4k.



Portrait of male old miner in coal shaft, dirty face, dark in the night.



Woman walking up a beach carrying a surfboard under her arm, long way brunette hair blows in the wind, wearing a wetsuit, long sleeves, morning sunlight reflects off the water, heavy surf.



A person in futuristic cyberpunk attire is taking steps on a planet surfaces made of vibrant, melting chocolate art. The person's reflection, distorted by neon city lights overhead, casts an eerie glow on the gooey terrain.



A large group of women are standing in a row, each wearing bright prison uniforms. They are lined up against a brick wall in a dimly lit room, their expressions varied from anxious to resigned. The atmosphere is tense and somber, with a sense of anticipation hanging in the air.



A photo of people drinking and laughing in a pub.



Beautiful pixel art of a street in Tokyo.



Interior photo of a messy room.



In a post-apocalyptic world, a German Shepherd dog wearing a bulky space suit lies amidst vibrant debris and rubble. Dramatic cinematic lighting highlights the vivid and sparkling colors of the destroyed landscape. The large breed dog seems alert yet calm, positioned between two large pieces of wreckage.



A woman with sprawling, vibrant red hair, the cover image of an editorial spread in Vogue, is situated in the center of an intricate abstract mixed media collage. Surrounding her, expressive shapes and bold lines of sacred geometry dance and intertwine, forming an intriguing and captivating background.



In a delightful claymation scene, a quirky and intricately detailed world comes to life under low key lighting. A small, round clay figure dressed in a white top hat and red bowtie gleams with the warm, soft glow as it dangles a string from its hand. The other end of the string gently touches the tip of a vibrant sunflower, its petals bursting with energy and character, basking in the muted yet inviting light. A curious ant, armed with a tiny backpack, cautiously wanders around the base of the sunflower, admiring the intricacies of its structure while the other anthropomorphic insects busily work around the bustling clay diorama, adding to the captivating and chaotic beauty of existence. Embrace the joy, the wonder, and the ceaseless whimsy that awaits in this warm, textured, and whimsical claymation scene.



Beautiful scene with mountains and rivers in a small village.



Macro photography of a miniature little village on top of a flower.



Cartoon characters, mini characters, figures, illustrations, flower fairy, green dress, brown hair, curly long hair, elf-like wings, many flowers and leaves, natural scenery, golden eyes, detailed light and shadow, a high degree of detail.

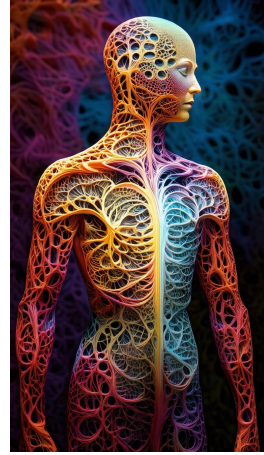
Figure 9. Text-to-1K image generation results produced by our Hydra-Transformer Hybrid model. The images are in resolutions 768×1344 and 1344×1344 . Please zoom in for clearer visualization.



Moonlight Maiden, cute girl in school uniform, long white hair, standing under the moon, celluloid style, Japanese manga style.



A space elevator, cinematic scifi art.



Human life depicted entirely out of fractals.



Shot in the style of a DSLR camera with the polarizing filter. A photo of two hot air balloons floating over the unique rock formations in Cappadocia, Turkey. The colors and patterns on these balloons contrast beautifully against the earthy tones of the landscape below. This shot captures the sense of adventure of enjoying such an experience.



Macro photography of a drop in the shape of a water cat. The photo has professional lighting and pastel colors. The surface of the water is reflective and the smooth blurred background helps the drop stand out.



Atmosphere, flat painting illustration, illustration, unique tall buildings in the city, irregular design, iron age, black and orange, detailed light and shadow, cyberpunk, technological age, high detail, CG feeling.



An intricate scene where a single drop of water, magnified, contains an entire miniature ecosystem. Inside the drop, a tropical forest filled with a green frog, tiger lilies, beautiful.



A propaganda poster depicting a cat dressed as french emperor napoleon holding a piece of cheese.



A Chinese model is sitting on a train, magazine cover, clothes made of plastic, photo realistic futuristic style, gray and green light, movie lighting 32K HD.

Figure 10. Text-to-1K image generation results produced by our Hydra-Transformer Hybrid model. The images are in resolutions 1344×768 . Please zoom in for clearer visualization.



A weathered, wooden mech robot covered in flowering vines stands peacefully in a field of tall wildflowers, with a small bluebird resting on its outstretched hand.

Digital cartoon, with warm colors and soft lines. A large cliff with a waterfall looms behind.



Female character wearing goggles while sitting in the desert, in the style of cyberpunk imagery, realistic hyper-detailed portraits, womancore, metallic accents, outrun, hyper-realistic pop, angelcore



A beautiful woman dressed in a dress made of autumn leaves in the forest, photography, natural lighting, high detail.



A portal into a mythical forest on the wall of my small messy bedroom.



The pink bunny girl in the cyber world is a cyberpunk, with beautiful long hair, wearing a pink skirt, pink bunny ears, pink headphones, neon lights, and a sense of technological future.



The Caped Crusader, Gotham skyline, rooftop, mysterious, powerful, nighttime, mixed media, expressionism, dark tones, high contrast, in the style of comic book artist Frank Miller, modern, gritty and textured, collage technique.



A dog and a cat playing on a beautiful beach.



A huge tree made out of pastel colored cotton candy; with blur on the background and space to use it for backgrounds, wallpapers, posters, banners.

Figure 11. Text-to-2K image generation results produced by our Hydra-Transformer Hybrid model. The images are in resolutions 1440×2560 . Please zoom in for clearer visualization.



Pirate ship trapped in a cosmic maelstrom nebula, rendered in cosmic beach whirlpool engine, volumetric lighting, spectacular, ambient lights, light pollution, cinematic atmosphere, art nouveau style, illustration art artwork by Senseijaye, intricate detail.



Furry character, character design, impasto, cute fox girl, long brown hair, curly long hair, fluttering in the wind, messy, big eyes, smile, petals fluttering in the wind, high detail, CG characters.



3D animation of a small, round, fluffy creature with big, expressive eyes explores a vibrant, enchanted forest. The creature, a whimsical blend of a rabbit and a squirrel, has soft blue fur and a bushy, striped tail. It hops along a sparkling stream, its eyes wide with wonder. Flowers that glow and change colors, trees with leaves in shades of purple and silver, and small floating lights that resemble fireflies. The creature stops to interact playfully with a group of tiny, fairy-like beings dancing around a mushroom ring.



A cute orange kitten sliding down an aqua slide, happy excited. 16mm lens in front. we see his excitement and scared in the eye. vibrant colors. water splashing on the lens.



A summer view of waterfall with pagodas and rocks.



An old rusted robot wearing pants and a jacket riding skis in a supermarket.

Figure 12. Text-to-2K image generation results produced by our Hydra-Transformer Hybrid model. The images are in resolutions 2560×1440 . Please zoom in for clearer visualization.



This dreamlike digital art captures a vibrant, kaleidoscopic bird in a lush rainforest.



A majestic gate in the middle of a mountain, 16k, high quality, best quality, style of a 3A game, fantastic style.



Photography closeup portrait of an adorable rusty breakdown steampunk robot covered in budding vegetation, surrounded by tall grass, misty futuristic sci-fi forest environment.



Cartoon characters, mini characters, hand-made, illustrations, robot kids, color expressions, boy, short brown hair, curly hair, blue eyes, technological age, cyberpunk, big eyes, cute, mini, detailed light and shadow, high detail.



Professional photograph of a lynx lit by moody harsh lighting in the middle of a forest.



A playful and endearing polar bear cub, its fluffy white fur standing out against a snowy backdrop. It wears a cozy knit cap and scarf, handcrafted with bright, cheerful colors to brave the winter chill. The bear's innocent eyes exude warmth and curiosity.

Figure 13. Text-to-2K+ image generation results produced by our Hydra-Transformer Hybrid model. The images are in resolutions 2560×2560. Please zoom in for clearer visualization.

C. Prompts of Figure 1

We provide the prompts for generating the images presented in Figure 1 here. In a raster scan order:

1. A dog that has been meditating all the time.
2. In a surreal office setting during a sunlit day, a man in a bizarre jelly mask, reminiscent of an oyster shell, occupies a full shot. He is seated at an office desk, his melancholic expression in contrast to the elaborate facades of yttrium yellow and zircon blue surrounding him.
3. Full-body photograph of a beautiful female cyborg, suspended in a worn-out, cassette-futurism science lab. The scene exudes a gritty retro sci-fi aesthetic from the 70s and 80s, with outdated technology and weathered machinery. Dust particles float in the light, enhancing the vintage, worn-down atmosphere. The cyborg's synthetic skin is torn from her down to her, revealing a complex but aged, metallic structure beneath. Her damaged breasts and partially exposed torso show signs of wear, with cracks and rust adding to the dystopian feel. Her body hangs lifeless from flickering, illuminated cords connected to her back.
4. A bouquet of roses made of pastel ice crystals.
5. A cat drinking a beer.
6. Paper artwork, layered paper, colorful Chinese dragon surrounded by clouds.
7. Beautiful neon lights forming the words "Hydra", glowing vibrantly.
8. Filmic photo of a group of three women on a street downtown, they are holding their hands up the camera.
9. A pink bunny girl in the cyber world, with beautiful long hair, wearing a pink skirt, pink bunny ears, pink headphones. Neon lights, and a sense of technological future.
10. Half human, half robot, repaired human, human flesh warrior, mech display, man in mech, cyberpunk.
11. Elephant amigurumi walking in savanna, a professional, blurry background.
12. Polychrome particles and powders surrounding a whimsical child figure silhouette emerging out of a portal.
13. A very cute little Shamrock bird in a mossy forest.